The Effect of Erosion on the Electrochemical Properties of AISI 1020 Steel

Jianhui Xie, Ahmet T. Alpas, and Derek O. Northwood

(Submitted 24 October 2002; in revised form 13 November 2002)

The mechanisms and characteristics of the mechano-electrochemical effect were investigated for eroded AISI 1020 steel specimens. The effect of erosion on open-circuit potential, corrosion potential, linear polarization resistance, and corrosion rate was determined. The corrosion rate was exponentially related to the decrease in corrosion potential and increase in the strain energy. The corrosion rate was quantitatively calculated using a mechano-electrochemical dynamic equation, which is based on the decrease in corrosion potential and increase in strain energy. The calculated rate agrees well with the experimentally measured corrosion rate.

Keywords corrosion, corrosion rate, electrochemical properties, erosion, mechano-electrochemical effect

1. Introduction

The mining industry encounters many problems due to the combined effects of corrosion and wear.[1-4] In ore grinding operations, the steel balls or rods suffer a considerable amount of wear. Wet grinding is preferred to dry grinding since it increases efficiency. However, the metal loss in wet grinding is several times that in dry grinding. This is the result of synergistic effects between abrasion, erosion, impact, and corrosion, but the mechanism of synergistic effect has not been well understood.[5-7]

The wear and corrosion processes involve many mechanical and electrochemical mechanisms, the combined actions of which often result in a significant increase in material degradation. The interactions among abrasion, rubbing, impact, and corrosion can significantly increase total material losses, especially in an aqueous environment, thereby producing a synergistic effect.[8-10] The synergistic effect is quite pronounced for the carbon steels.

The synergistic effect is a result of a mechano-electrochemical effect. The mechano-electrochemical effect is defined as the influence of plastic deformation on the electrochemical properties.[11-13] The mechano-electrochemical effect would be present in an environment comprised of both mechanical action (causing deformation) and a corrosive agent.

In this study, the mechano-electrochemical effect due to dry erosion followed by corrosion was determined for an AISI 1020 steel. The electrochemical properties that were measured included the open-circuit potential, polarization resistance, Tafel slopes, and corrosion rates. The change in electrochemical behavior was related to the change in stored energy produced by erosion.

Jianhui Xie, **Ahmet T. Alpas**, and **Derek O. Northwood,** Engineering Materials, University of Windsor, 401 Sunset Avenue, Windsor, Ontario Canada N9B 3P4. Contact e-mail: dnorthwo@uwindsor.ca.

2. Experimental Details

2.1 Material and Test Specimens

The material used in this study was an AISI 1020 steel with a chemical composition of (wt.%): 0.20 C, 0.60-0.90 Mn, 0.04 max P, 0.05 max S, and balance Fe.

The specimens were in the form of plates with dimensions: 50 mm in length, 25 mm in width, and 3 mm in thickness. They were polished using abrasive papers #180 to #600 before heat-treatment.

For annealing, the specimens were placed in a furnace at 870 °C and heated for 1 h, then furnace-cooled to room temperature. For quenching, the specimens were immersed into water after being heated 1 h at 900 °C in the furnace. The heavy scale produced during heat-treatment was removed using a plastic plate, and the specimens were then pickled in a hydrochloric acid solution (50% HCl and 50% water) for 30 min. The pickled specimens were then thoroughly rinsed in water and dried to prevent corrosion prior to electrochemical testing.

The hardnesses of the heat-treated and as-received specimens are given in Table 1. The microstructures of the as-received, annealed, and quenched specimens are shown in Fig. 1(a-c). The as-received specimen microstructure consisted of carbides and pearlite in a matrix of ferrite, with elongated grains. The annealed specimen had a pearlite structure and the grains were equiaxed and larger than as-received. The quenched specimen had a plate-like martensite structure. There was no decarburized layer in the heat-treated specimens; the decarburized layer is removed by the pickling treatment.

2.2 Erosion Testing

Dry erosion testing was carried out in a customized erosion tester, shown schematically in Fig. 2. The erodent (SiC particles, 120 grit size) is carried along a steel pipe by pressurized

Table 1 Hardness of Heat-Treated and As-Received 1020 Steel

1020 Steel	As-Received	Annealed	Quenched
Hardness	23HRC	67HRB	40HRC

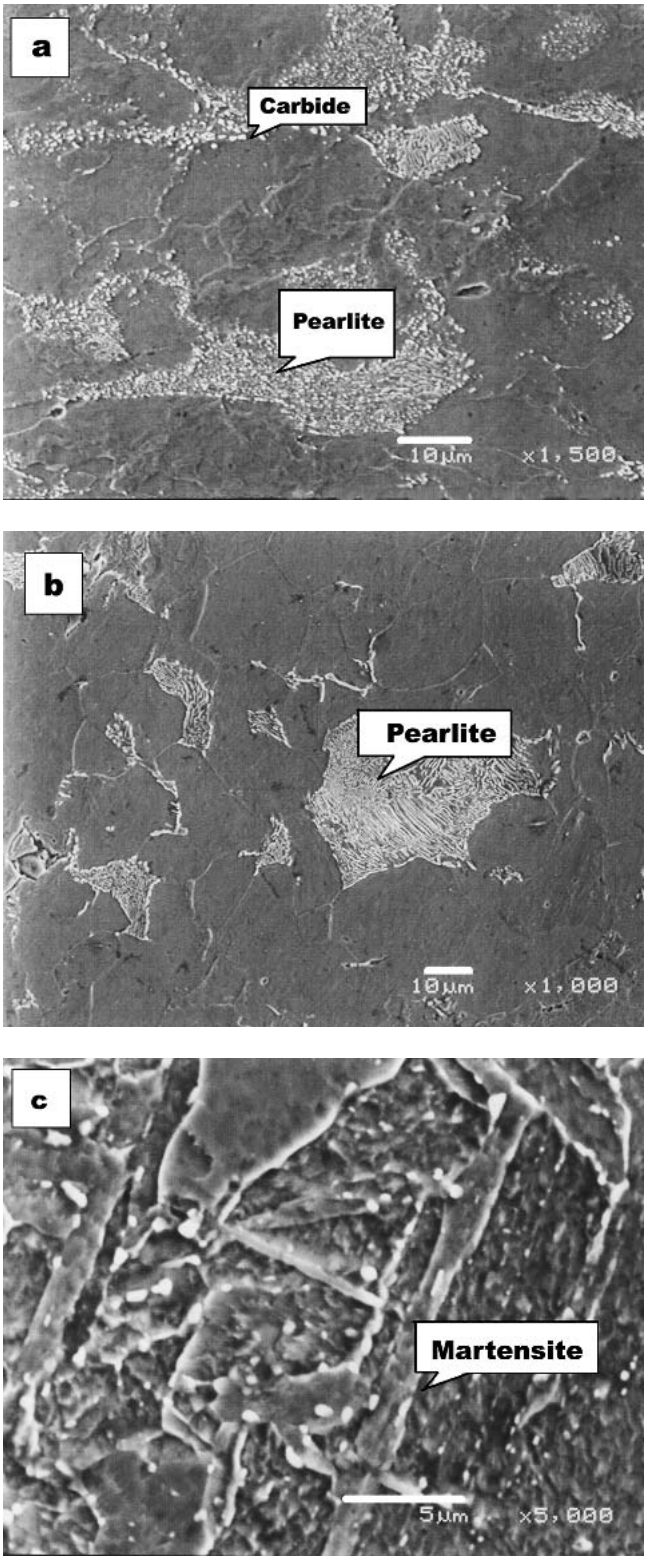

Fig. 1 SEM micrographs of **(a)** as-received, **(b)** annealed, and **(c)** quenched AISI 1020 specimens

air to impact on the steel specimen at a velocity of 38 m/s.[14] The amount of erodent was 0 g (i.e., uneroded), 10 g, 50 g, and 100 g. The erosion angle was set at 45°.

2.3 Electrochemical Measurements

Electrochemical measurements were conducted in a solution of 2 g/L NaCl and 2 g/L Na_2SO_4 (adjusted to neutral pH value) using a Solartron 1285 Potentiostat/Galvanostat (Solartron Group Ltd; Farnborough, UK) and CorrView software (Scribner Associates, Inc., Charlottesville, VA), and a tri-electrode cell. The eroded/uneroded specimens were used as the working electrodes (WE). A saturated calomel electrode (SCE) was used as the reference electrode (RE) and a graphite plate was used as the counter electrode (CE).

The electrochemical measurements were made for the eroded specimens immediately after the erosion test (the eroded surface was first blown clean by pressurized air). The specimens were sealed using waterproof adhesive tape to expose only a small, eroded area (about 0.5-1.0 cm^2, used to calculate the current density by dividing the current by the area) of the specimen to the solution and to protect the connecting clips.

The measured electrochemical parameters included the open-circuit potential, the polarization resistance, R_p, determined by linear polarization measurements (polarized from –10 mV to +10 mV, versus open-circuit potential on the specimen), and the Tafel slopes b_a and b_c determined from potentiodynamic polarization measurements (polarized from –300-600 mV, versus open-circuit potentials on the specimen). The corrosion rate was then calculated by dividing the constant B (calculated from Tafel slopes) by the polarization resistance, R_p.

2.4 Microstrain Measurement

X-ray diffraction (XRD) analysis was used to characterize the microstrain induced in the steel by the impact of the SiC particles. The corresponding stored strain energy can be calculated from this microstrain.

The microstrain due to erosion can be calculated from the broadening of the XRD peak. The broadening is determined by measuring the width B, in radians, at an intensity equal to half the maximum intensity. If the observed X-ray peak of the eroded specimen has a width B_o, and the width due to instrumental effects (determined by the peak broadening of a fully annealed specimen) is B_i, then the remaining width, B_r, is due to the combined effects of crystallite size and microstrain

$$B_r = \sqrt{B_o^2 - B_i^2} \quad \text{(Eq 1)}$$

According to Suryanarayana and Norton[15]

$$B_r \cos\theta = \frac{k\lambda}{L} + \eta \sin\theta \quad \text{(Eq 2)}$$

where k is a constant, λ is the wavelength of x-rays, L is the average crystallite size, and η is the microstrain. The microstrain, η, can be obtained from the slope of the plot of $B_r\cos\theta$ versus $\sin\theta$.

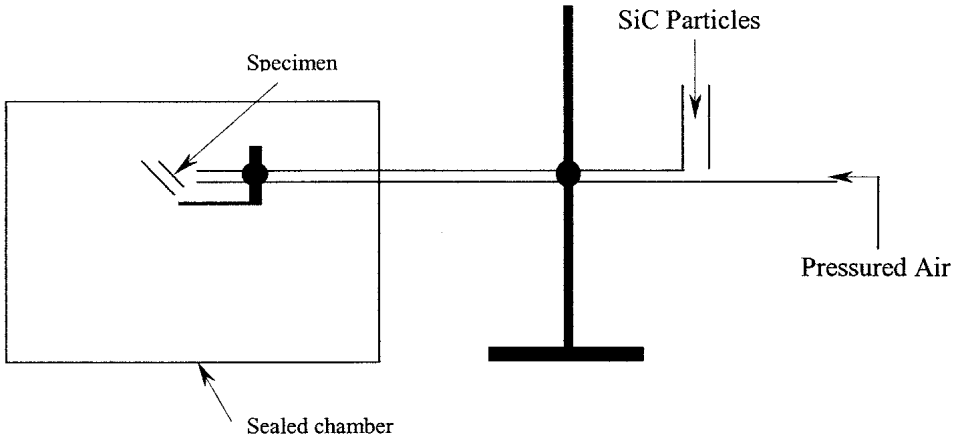

Fig. 2 Schematic diagram of customized erosion tester

3 Results and Discussion

3.1 The Effect of Erosion on Open-Circuit Potential

Figure 3(a-c) shows the effect of erosion on the open-circuit potentials for the as-received, annealed, and quenched specimens after −10mV (versus open-circuit potential) overpotential polarization on the specimen. The open-circuit potentials initially shift a small amount in a positive direction, which is a result of recovery from the negative polarization, then shift negatively or positively at a relatively small rate of change. The electrochemical reactions during cathodic polarization dissolve the porous oxides on the surface, resulting in a fresh and active surface. Thus, the open-circuit potentials are almost constant with time. An oxide film comprised of Fe_3O_4 and FeOH is formed on the surface when the specimens are immersed in the corrosive solution. The FeOH is a porous and nonprotective film. While the overpotential of –10 mV (versus open-circuit potential) is a very small amount of polarization, the porous oxide may be dissolved completely, the tightly adherent oxide (very thin) protects the surface, and thus the open-circuit potential increases a relatively small amount. If the small amount of negative polarization is not enough to dissolve the porous oxide film completely, a galvanic electrochemical cell is formed between the steel matrix and the iron oxides. This leads to a high electrochemical activity and the open-circuit potential shifts a very small amount in a negative direction.

The open-circuit potentials of the eroded specimens were displaced in a negative direction, i.e., were lower than that of the uneroded specimens. Furthermore, the open-circuit potential became more negative with increasing amount of erodent. The open-circuit potentials of the eroded specimens at the 10 min measurement period are given in Table 2 and compared with the open-circuit potentials of the uneroded specimens.

The relationship between the open-circuit potential and the amount of erodent is shown in Fig. 4. For all specimens, the open-circuit potentials shift in a negative direction with increasing amount of erodent. Because the open-circuit potential is a thermodynamic parameter, which is associated with the free energy of the electrochemical reaction, the lower the electrochemical potential, the lower the free energy is and thus the electrochemical reaction is enhanced. It is thus concluded that erosion, which causes a negative shift in the open-circuit potential, thermodynamically facilitates the corrosion reaction on the eroded surface of the specimen.

3.2 Electrochemical Kinetics of Eroded Specimens

The relationship between the polarization current, I, and the electrode potential, E, can be expressed as in Eq 3 when the corrosion reaction is controlled by active polarization.[16]

$$I = i_k \left\{ \exp\left[\frac{2.303(E - E_k)}{b_a}\right] - \exp\left[\frac{2.303(E_k - E)}{b_c}\right]\right\} \quad \text{(Eq 3)}$$

where E_k is the corrosion potential, i_k is the corrosion rate when the external current density is zero, and b_a and b_c are the anodic and cathodic Tafel slopes. When only a small overpotential is applied to the electrode, Eq 3 can be simplified as follows[16]:

$$i_k = \frac{b_a b_c}{2.303(b_a + b_c)} \cdot \left(\frac{\Delta E}{\Delta I}\right)^{-1} \quad \text{(Eq 4)}$$

The term $\Delta E/\Delta I$ is defined as the polarization resistance, R_p. The term $b_a b_c/2.303(b_a + b_c)$ is a constant and is expressed as B. Thus the corrosion rate can be related to the polarization resistance, R_p, as follows:

$$i_k = \frac{B}{R_p} \quad \text{(Eq 5)}$$

The polarization resistance, R_p, combined with the capacitance of the double layer, determines the current density (corrosion rate). Thus the polarization resistance, R_p, is a very important kinetic parameter and can be determined, based on its definition, from the slope of the linear polarization curves. Linear polarization curves are shown in Fig. 5(a-c) for the as-received, annealed, and quenched specimens, respectively. The deviation of actual data from the simulated linear relationship, expressed by mean-square error, R^2, is almost equal to 1, illustrating that the actual data fall very close to the linear line. The intersection at the overpotential axis when polarization current density is zero is at the order of magnitude of –19, showing that the

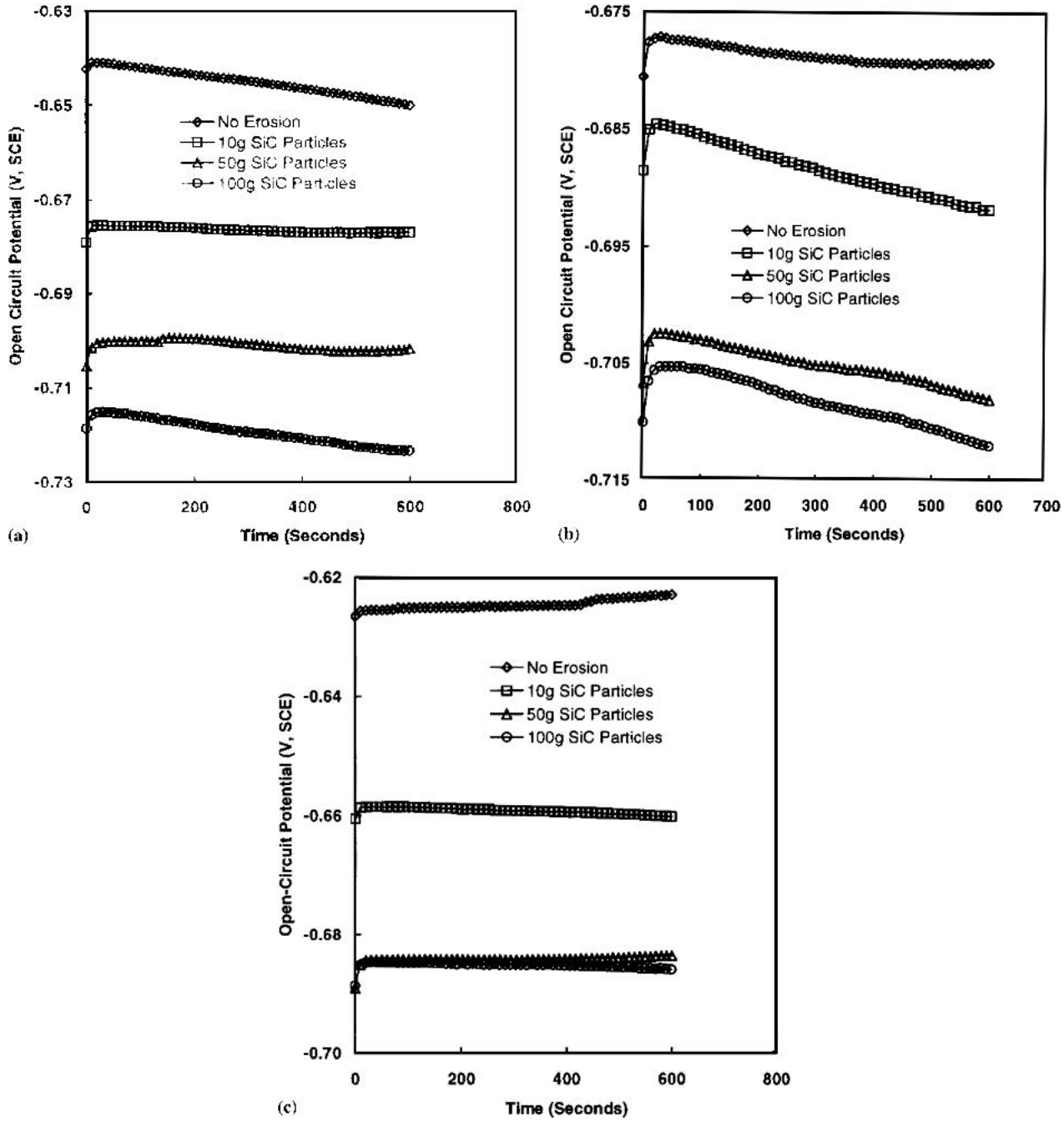

Fig. 3 Open-circuit potential versus time for **(a)** as-received, **(b)** annealed, and **(c)** quenched AISI 1020 steel

deviation of the linear lines from the origin is very small (i.e., the linear plots essentially pass through the origin).

The polarization resistances of the as-received, annealed, and quenched specimens after erosion are lower than the uneroded specimens, and the polarization resistance decreases with an increasing amount of erodent. According to Eq 5, a lower polarization resistance indicates a higher corrosion rate. Thus, erosion kinetically increases the corrosion and the corrosion rate increases with an increasing amount of erodent.

The Tafel slopes, b_a and b_c, and corrosion potential can be obtained from the potentiodynamic polarization curves. The Tafel slopes were obtained using the CorrView software on the Solartron 1285 potentiostat. Potentiodynamic polarization curves are shown in Fig. 6(a-c) for the as-received, annealed, and quenched specimens, respectively. A summary of the electrochemical parameters obtained from the linear polarization and potentiodynamic polarization measurements is given in Table 3.

Each of the polarization curves has an anodic and cathodic polarization portion. There is a limiting current in the cathodic polarization curve. In the cathodic reaction, transportation of ions is the controlling step for which the corrosion takes place

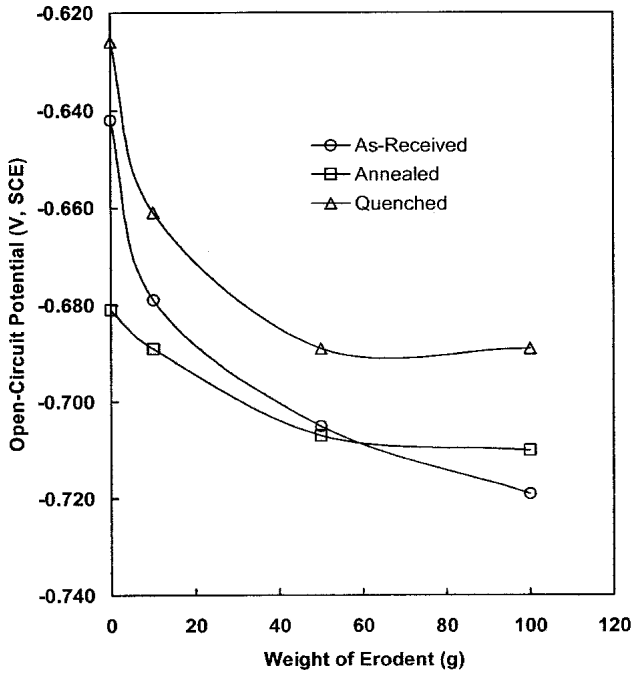

Fig. 4 Effect of erosion on the open-circuit potential

Table 2 Open-Circuit Potentials of Eroded and Un-Eroded Specimens

	Open-Circuit Potential (V, SCE)			
Heat-Treatment	Uneroded	10 g Erodent	50 g Erodent	100 g Erodent
As-received	–0.642	–0.679	–0.705	–0.719
Annealed	–0.681	–0.689	–0.707	–0.710
Quenched	–0.626	–0.661	–0.689	–0.689

at a steady rate, which is equivalent to the transportation rate of corrosive agent ions. Compared with the uneroded specimen, the entire polarization curves for the eroded specimens are shifted downward (i.e., more negative potentials), and at the same time shift to the left side (i.e., lower current densities). The limiting current gradually disappears (i.e., the concentration-controlled reaction gradually converts to an activation-controlled one). From the intersection of anodic and cathodic polarization curves, the corrosion potential is obtained and is found to move in a negative direction with increasing erosion.

It is concluded from the downward movement of the polarization curves that the eroded specimens have a higher corrosion rate (higher polarization current) if all the specimens are subjected to a same polarization potential. The anodic reactions (corrosion reaction) take place more easily for the eroded specimens due to the more negative corrosion potentials. Thus, the corrosion reactions on the eroded specimens are accelerated in terms of kinetics (corrosion rate) and thermodynamics (corrosion potential). The polarization curve is critical to the evaluation of the corrosion reaction characteristics from both a kinetic and thermodynamic point of view.

Due to erosion, which causes plastic deformation, the electrochemical parameters are affected differently. The polarization resistance decreases and the open-circuit potential and corrosion potential shift in a negative direction. With an increasing amount of erodent, the polarization resistance of eroded specimens decreases (see Fig. 7) and from Eq 5, the corrosion reaction thus takes place at a higher rate. From a thermodynamic point of view, more negative corrosion potential also facilitates the corrosion reaction. Thus, increasing erosion favors the corrosion reaction dynamically and thermodynamically (Fig. 8).

3.3 The Microstrain Induced by Erosion

The XRD peak positions remain almost constant at the same angular positions for the different erosion conditions. There is, however, x-ray peak broadening for all eroded specimens and the amount of broadening increases with an increasing amount of erodent.

Based on the measured x-ray peak broadening, and using a multiple order reflections method[17,18] (<110> and <220>), $B_r \cos\theta$ was plotted against $\sin\theta$. The slope of this plot is defined as the microstrain cumulated in the eroded specimens. The microstrains in the <110> direction calculated from the broadening are given in Table 4(a). Due to cold work and distortion from heat treatment, a small amount of residual microstrain exists in the as-received and quenched specimens. The "extra" microstrain induced by erosion is given in Table 4(b). The microstrain increases with an increasing amount of erodent regardless of heat treatment; this is the result of increased plastic deformation due to erosion. The microstrain produced by erosion is different for the annealed, as-received, and quenched specimens; this is possibly due to the fact that there are different microstructures and different hardnesses in heat-treated and as-received samples; thus the deformation mechanism is possibly different.

3.4 Stored Stain Energy in Eroded Specimens

As a result of plastic deformation, the deformed metals absorb energy. Thus, the deformed specimen has a higher electrochemical activity, and the potential of the deformed electrode will, therefore, shift in a negative direction (Table 2).

Plastic deformation will produce an increase in stored energy. This stored strain energy can be calculated from the microstrain, using the following equation[17,18]:

$$A = \frac{15E}{2(3 - 4u + 8u^2)} \cdot \left(\frac{\Delta d}{d}\right)^2 \qquad \text{(Eq 6)}$$

where A is the stored strain energy, E is Young's modulus (92.4×10^9 N/m^2 for AISI 1020 steel), $\Delta d/d = 2\eta$ and u is Poisson's ratio (0.33 for AISI 1020 steel). The calculated stored strain energies for the eroded specimens are given in Table 5.

The stored strain energy increases with increase in the amount of erodent for the three different heat-treatments. There is some level of residual strain energy for the as-received and quenched specimens due to cold working or distortion from the heat-treatment. All the stored strain energy of annealed AISI 1020 steel comes from the erosion. The increased strain energy

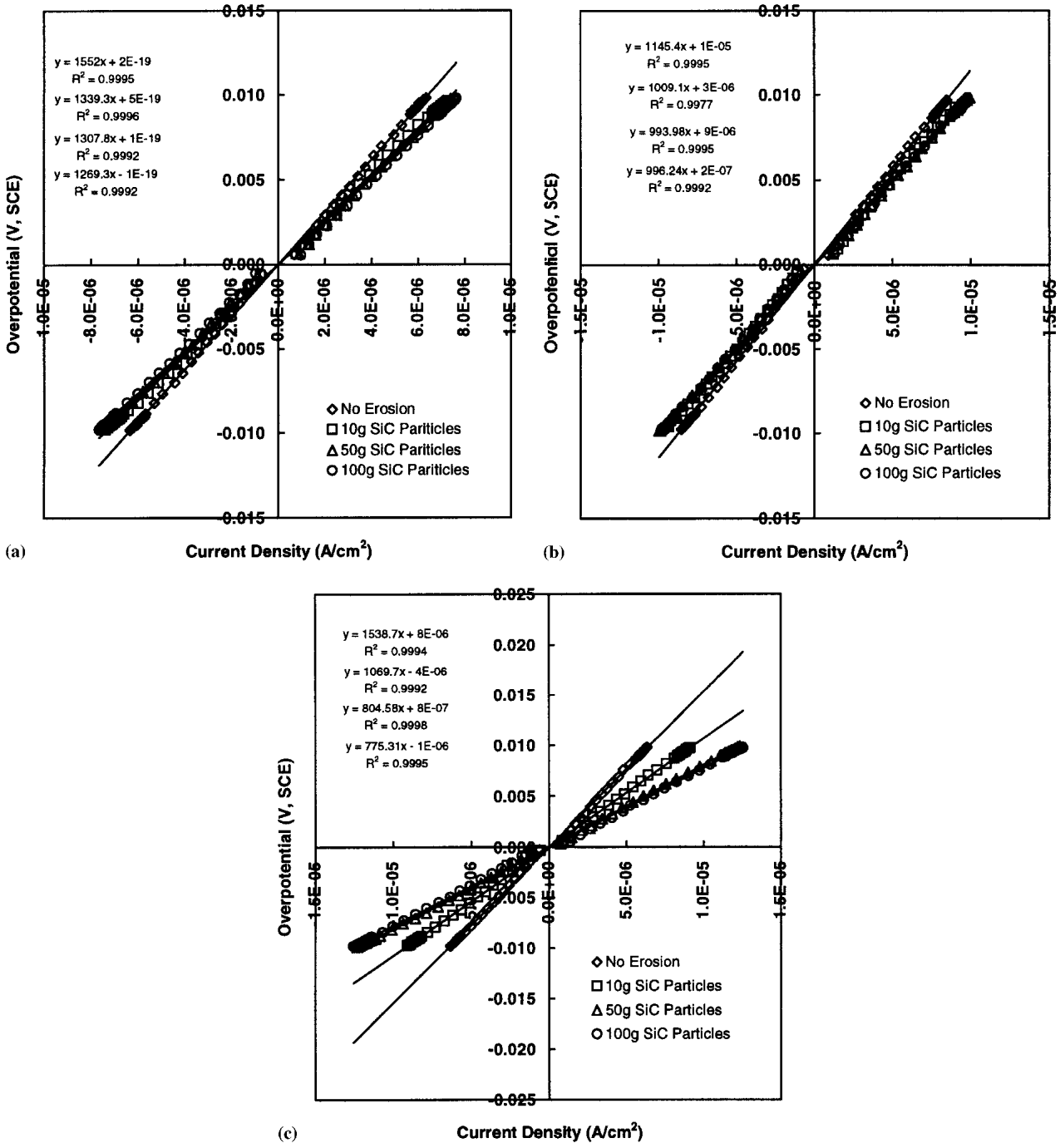

Fig. 5 Linear polarization curves for **(a)** as-received, **(b)** annealed, and **(c)** quenched AISI 1020 steel

gives rise to increased chemical and electrochemical activity of the eroded specimens and the corrosion rate increases.

3.5 Mechanisms for Accelerated Corrosion Due to Erosion

Due to the plastic deformation of the surface caused by erosion, the deformed surface is electrochemically activated and the corrosion reaction of the deformed surface is accelerated. The accelerated corrosion reaction is reflected in the negative shift in open-circuit potential and corrosion potential, decrease in polarization resistance, increase in microstrain, and stored strain energy. The relation can be expressed by the following equation[14]:

$$i_A^s = i_A e^{\frac{\Delta E_k}{b_a}} e^{\frac{A}{RT}} \quad \text{(Eq 7)}$$

where i_A^s is the corrosion rate of eroded specimens; i_A the

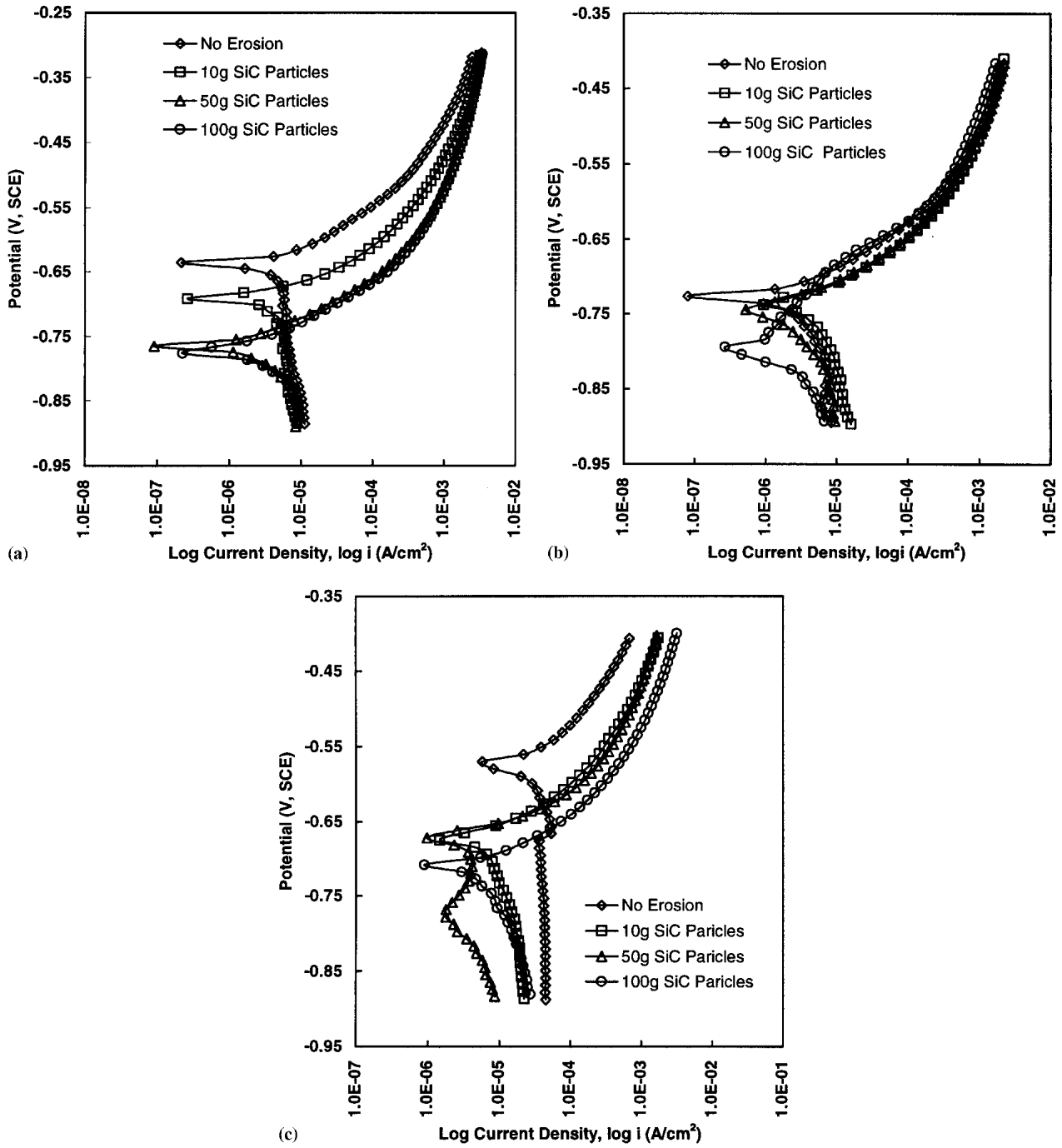

Fig. 6 Potentiodynamic polarization curves for **(a)** as-received, **(b)** annealed, and **(c)** quenched AISI 1020 Steel

corrosion rate of uneroded specimens; ΔE_k the decrease in the corrosion potential; b_a the Tafel slope of the anodic polarization curve; A the strain energy caused by erosion; R the gas constant; and T the temperature. Equation 7 demonstrates that the corrosion rate of eroded specimens is higher than for the uneroded specimens, because the term $\exp(\Delta E_k/b_a)*\exp(A/RT)$ is greater than 1. The increased corrosion rate is related to the thermodynamic parameters (ΔE_k and A) and the kinetic parameter (b_a). The corrosion rate is exponentially related to the decrease in corrosion potential and increase in the strain energy.

Figure 9 shows the relationship between the corrosion rate and the decrease in corrosion potential. The decrease in corrosion potential is the difference in corrosion potential between an eroded specimen and an uneroded specimen. The equations listed on the graph from top to bottom for the as-received, annealed, and quenched specimens show that the corrosion rate is exponentially related to the decrease in corrosion potential,

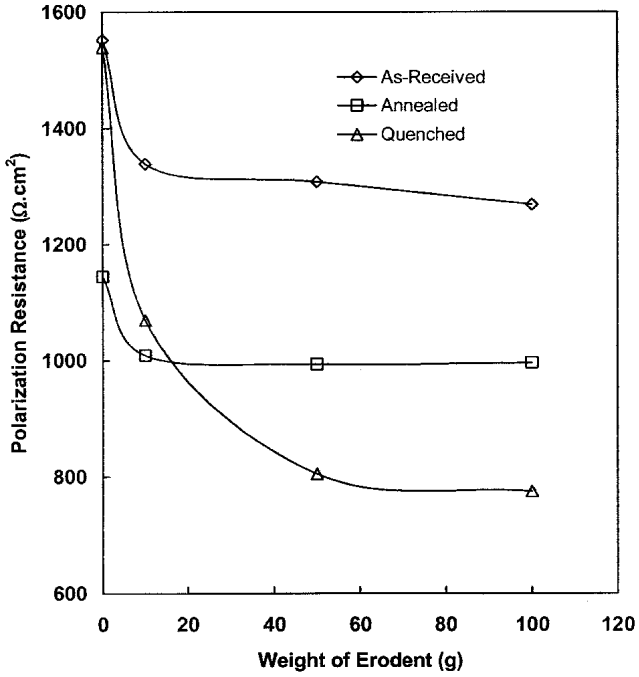

Fig. 7 Decrease in polarization resistance due to erosion

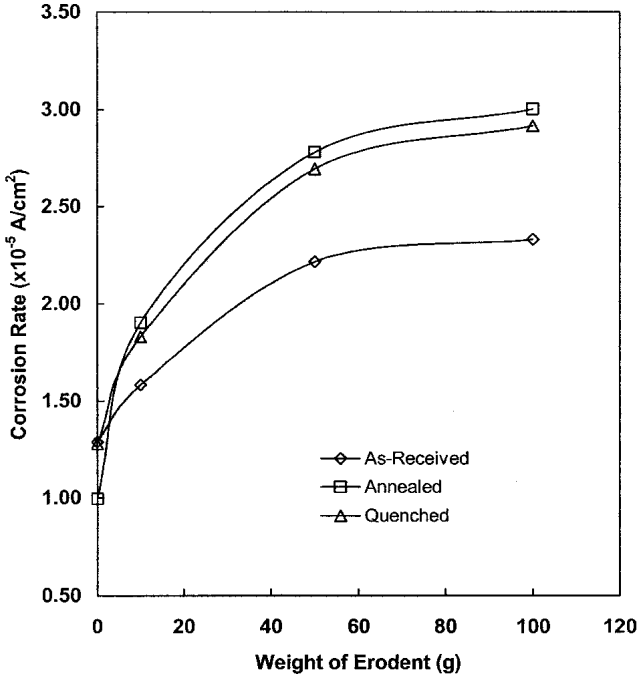

Fig. 8 Increase in corrosion rate due to erosion

Table 3 Electrochemical Parameters for the Eroded and Uneroded Specimens

Heat Treatment	Electrochemical Parameter		Value of Parameter: No Erosion	10 g Erodent	50 g Erodent	100 g Erodent
	Polarization Resistance ($\Omega \cdot cm^2$)		1552	1339	1308	1269
As-Received	Tafel Slopes	b_a (V)	0.061	0.059	0.076	0.077
		b_c (V)	–0.186	–0.288	–0.539	–0.588
		B	0.020	0.021	0.029	0.030
	Corrosion Potentials (V)		–0.636	–0.692	–0.765	–0.776
	Corrosion Rate ($\times 10^{-5}$ A/cm^2)		1.285	1.588	2.211	2.330
	Polarization Resistance ($\Omega \cdot cm^2$)		1145	1009	994	996
Annealed	Tafel Slopes	b_a (V)	0.029	0.064	0.064	0.105
		b_c (V)	–0.253	–0.145	–0.189	–0.191
		B	0.011	0.019	0.021	0.030
	Corrosion Potential (V)		–0.717	–0.738	–0.754	–0.784
	Corrosion Rate ($\times 10^{-5}$ A/cm^2)		0.987	1.911	2.780	2.954
	Polarization Resistance ($\Omega \cdot cm^2$)		1539	1070	805	775
Quenched	Tafel Slopes	b_a (V)	0.069	0.069	0.064	0.068
		b_c (V)	–0.133	–0.130	–0.225	–0.219
		B	0.020	0.020	0.022	0.023
	Corrosion Potential (V)		–0.570	–0.675	–0.672	–0.708
	Corrosion Rate ($\times 10^{-5}$ A/cm^2)		1.282	1.829	2.688	2.907

and the error expressed by R^2 is very close to one. The corrosion rate is also exponentially related to the strain energy accumulated during erosion (Fig. 10).

The calculated corrosion rates (using Eq 7) of AISI 1020 steel are given in Table 6. There is considerable difference between the experimental and calculated corrosion rates, based on a theoretical analysis, for the as-received and quenched specimens, while the difference for the annealed electrode is very small. If a graph of the calculated corrosion rate (using Eq 7) versus the experimental corrosion rate is plotted, there is a linear relationship (Fig. 11) for the annealed electrode with an error expressed by R^2 of 0.91. However, the linearity of the plots for the as-received and quenched electrodes is not as good as that for the annealed electrode. The possible reason is that the stored microstrain and strain energy for the annealed electrode arises only from erosion, while those for the as-received and quenched specimens are both from erosion and cold-working or heat treatment distortion. Thus Eq 7 is valid for the annealed electrode, where strain is produced only by erosion.

4. Conclusions

Due to erosion, the open-circuit potential shifts in a negative direction, which thermodynamically accelerates the corrosion.

The polarization resistance decreases with the increasing amount of erodent, which kinetically accelerates the corrosion reaction.

The corrosion rate, as calculated by linear polarization and potentiodynamic polarization measurements, increases with an increasing amount of erodent. The increased corrosion rate is exponentially related to the decrease in open-circuit potential and increase in stored strain energy for the annealed specimen, where the microstrain is only accumulated from erosion. The increased corrosion rate is a result of the plastic deformation caused by erosion.

The effect of erosion on the electrochemical parameters is

Table 4a Total Microstrain Measured in Specimens

Heat Treatment	Microstrain, $\times 10^{-3}$			
	No Erosion	10 g	50 g	100 g
As-Received	2.60	9.41	10.14	15.94
Annealed	0	10.89	14.35	15.26
Quenched	3.77	8.94	10.51	13.00

Table 4b "Extra" Microstrain Induced by Erosion

Heat Treatment	Microstrain, $\times 10^{-3}$		
	10 g	50 g	100 g
As-Received	6.81	7.54	13.34
Annealed	10.89	14.35	15.26
Quenched	5.17	6.74	9.23

Table 5 Stored Strain Energy

Heat Treatment	Strain Energy, J/mol			
	No Erosion	10 g Erodent	50 g Erodent	100 g Erodent
As-Received	52	684	794	1962
Annealed	0	916	1590	1798
Quenched	110	623	853	1305

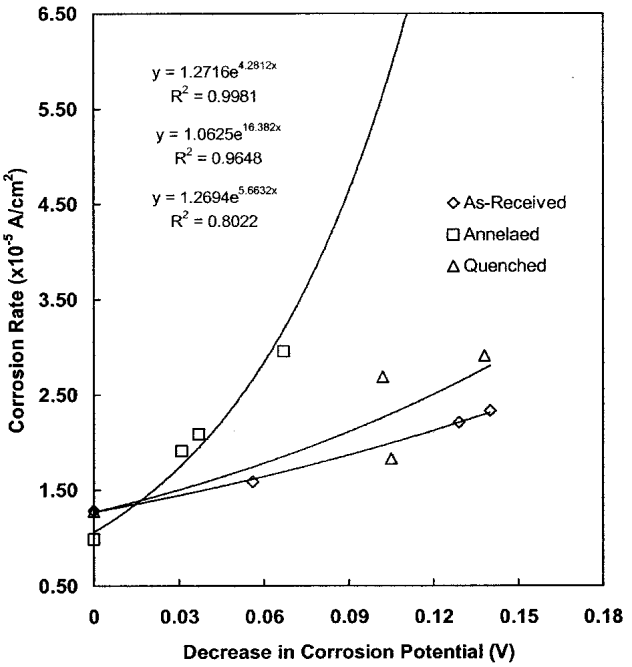

Fig. 9 Corrosion rate as a function of decrease in open-circuit potential

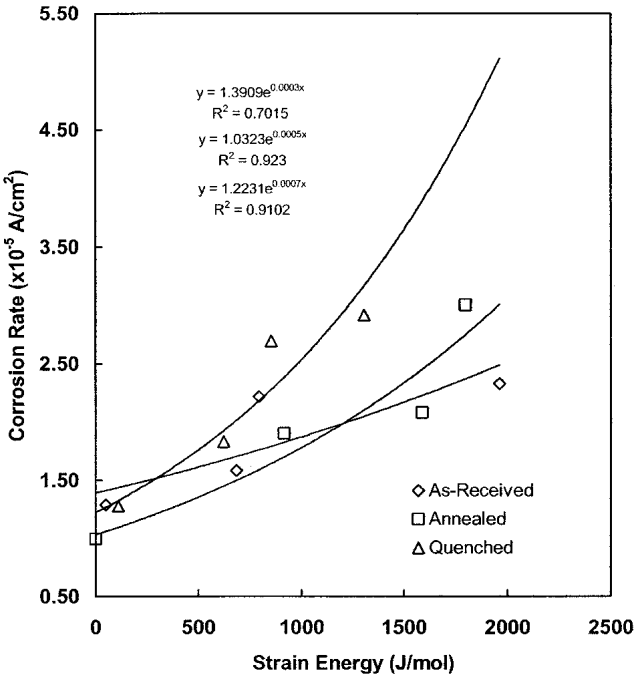

Fig. 10 Corrosion rate as a function of stored strain energy

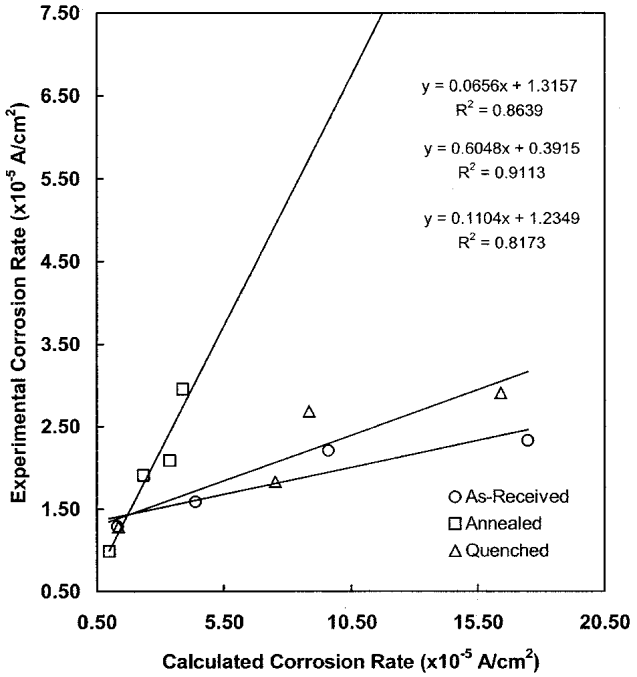

Fig. 11 The relationship between the calculated corrosion rate and the experimental corrosion rate

Table 6 Calculated and Measured Corrosion Rates of Eroded AISI 1020 Steel

AISI 1020 Steels	Corrosion Rate i_A^s	Corrosion Rate, $\times 10^{-5}$ A/cm^2 Amount of Erodent, Erosion Angle 45°			
		No Erosion	10 g	50 g	100 g
As-Received	Experimental corrosion rate	1.28	1.59	2.21	2.33
	Calculated corrosion rate	1.31	4.38	9.60	17.48
Annealed	Experimental corrosion rate	0.99	1.91	2.09	2.95
	Calculated corrosion rate	0.99	2.32	3.54	3.87
Quenched	Experimental corrosion rate	1.28	1.83	2.69	2.91
	Calculated corrosion rate	1.34	7.52	8.84	16.42

characterized by the mechano-electrochemical effect. The corrosion rate calculated theoretically from the equation for the mechano-electrochemical effect agrees well with the experimentally measured corrosion rate for the annealed specimen.

Due to the residual microstrain from the heat-treatments of the as-received and quenched specimens, the calculated corrosion rates deviate from the proposed mechano-electrochemical effect equation. Thus, more work needs to be done to characterize the corrosion rates of these two conditions using mechano-electrochemical effect.

References

1. A. Neville, T. Hodgkiess, and J.T. Dallas: "A Study of the Erosion-Corrosion Behavior of Engineering Steels for Marine Pumping Applications," *Wear*, 1995, *186-187*, pp. 497-507.
2. A. Fang, J. Long, and Z. Tao: "Failure Analysis of the Impeller of a Slurry Pump Subjected to Corrosive Wear," *Wear*, 1995, *181-183*, pp. 876-82.
3. J.H. Bulloch: "Electrochemical Potential Variations in a Small 40 MW Feedwater Storage Vessel—the Influence of Weldment Surface Condition," *Int. J. Pressure Vessels & Piping*, 1997, *71*, pp. 1-5.
4. T.C. Zhang, X.X. Jiang, and S.Z. Li: "Acceleration of Corrosive Wear of Duplex Stainless Steel by Chloride in 69% H_3PO_4 Solution," *Wear*, 1996, *199*, pp. 253-59.
5. A. Fang, J. Long, and Z. Tao: "An Investigation of the Corrosive Wear of Stainless Steels in Aqueous Slurries," *Wear*, 1996, *193*, pp. 73-77.
6. S.W. Watson, F.J. Friedersdrof, B.W. Madsen, and S.D. Cramer: "Methods of Measuring Wear-Corrosion Synergism," *Wear*, 1995, *181-183*, pp. 476-84.
7. M.K. Lee, W.W. Kim, C.K. Rhee, and W.J. Lee: "Investigation of Liquid Impact Erosion for 12Cr Steel and Stellite 6B," *J. Nucl. Mater.*, 1998, *257*, pp. 134-44.
8. A. Neville, T. Hodgkiess, and H. Xu: "An Electrochemical and Microstructural Assessment of Erosion–Corrosion of Cast Iron," *Wear*, 1999, *233-235*, pp. 523-34.
9. T. Hodgkiess, A. Neville, and S. Shrestha: "Electrochemical and Mechanical Interactions During Erosion–Corrosion of a High-Velocity Oxy-Fuel Coating and a Stainless Steel," *Wear*, 1999, *233-235*, pp. 623-34.
10. F. Assi and H. Bohni: "Study of Wear-Corrosion Synergy With a New Microelectrochemical Technique," *Wear*, 1999, *233-235*, pp. 505-14.
11. X.C. Lu, K. Shi, S.Z. Li, and X.X. Jiang: "Effects of Surface Deformation on Corrosive Wear of Stainless Steel in Sulfuric Acid Solution," *Wear*, 1999, *225-229*, pp. 537-43.
12. R. Akid and I. Dmytrakh: "Influence of Surface Deformation and Electrochemical Variables on Corrosion and Corrosion Fatigue Crack Development," *Fatigue & Fracture of Eng. Mater. & Structures*, 1998, *21*, pp. 903-11.
13. S.K. Varma and R.R. Romero: "The Effect of Impact and Continuous Scratches on the Corrosive Wear Behavior of Fe-18%Cr-5%Ni Alloy and 304 Stainless Steel for Two Grain Sizes," *Wear*, 1996, *201*, pp. 121-31.
14. J. Xie: "Characteristics and Mechanism of the Synergistic Effect Between Erosion and Corrosion," Ph.D. Dissertation, University of Windsor, Windsor, Ontario, Canada, 2001.
15. S.I. Rao and C.R. Houska: "The Measurement of Elastic Stresses and Energy in Cubic Single-Crystal Films by X-Ray Diffraction," *J. Appl. Phys.*, 1981, *52*(10), pp. 6322-27.
16. F. Mansfeld: "Tafel Slopes and Corrosion Rates From Polarization Resistance Measurements," *Corrosion*, 1973, *29*(10), pp. 397-402.
17. D.O. Northwood: "The Effect of Mechanical Deformation on Selected Chemical and Physical Properties of Crystalline Solids," Ph.D. Dissertation, University of Surrey, UK, 1968.
18. D. Lewis, D.O. Northwood, and C.E. Pearce: "A Study of the Effects of Microstrain on the Electrode Potential and the Anodic Dissolution of Cu," *Corrosion Sci.*, 1969, *9*, pp. 779-87.